Optics & Laser Technology 157 (2023) 108650

Contents lists available at ScienceDirect

Optics and Laser Technology

journal homepage: www.elsevier.com/locate/optlastec

Full length article

Bend-resistant high-resolution imaging optical fiber

Fei Qu [a,b,1], Bingsheng Xu [a,b,1], Fei Yu [a,c,*], Fei Li [d], Xin Lin [d,*]

[a] Key Laboratory of Materials for High Power Laser, Shanghai Institute of Optics and Fine Mechanics, Chinese Academy of Sciences, Shanghai 201800, China
[b] Center of Materials Science and Optoelectronics Engineering, University of Chinese Academy of Sciences, Beijing 100049, China
[c] Hangzhou Institute for Advanced Study, University of Chinese Academy of Sciences, Hangzhou 310024, China
[d] State Key Laboratory of High-Temperature Gas Dynamics, Institute of Mechanics, Chinese Academy of Sciences, Beijing 100190, China

ARTICLE INFO

Keywords:
Fiber fabrication
Imaging optical fiber
Fiber bundle
High resolution
High NA
Bend-resistant

ABSTRACT

We report design, fabrication, and characterization of bend-resistant high-resolution imaging optical fiber comprising over five thousand cores. The fiber is made of low-cost commercial-available H-ZK9B and H-K3 glasses which gives rise to a maximum numerical aperture up to 0.552 at 750 nm wavelength. The multi-stacking arrays of three-sized cores can effectively suppress the core-to-core crosstalk and raise the bend resistance. No degradation of imaging is demonstrated at a bending radius less than 2 cm and at an extensive wavelength range from the visible to the near-infrared, showing a substantial improvement over commercial state-of-the-art fiber bundles.

1. Introduction

Fiber endoscope technology emerged at the early stage of optical fiber development and is now playing an inevitable role in biomedical imaging and many applications where a lightweight and miniaturized imaging system is required [1]. Multi-core imaging fiber (MCIF)/fiber bundle, as a key element of endoscopy, usually comprises thousands of cores or more that spatially sample the incident light field and delivery to the distal end. Today bonding with deep learning and computational imaging methods, the imaging through MCIF is exploiting the potential to circumvent its physical limits [2,3] (see Table 1).

Direct-stacking [4], chemical-leaching [5] and stacking-and-draw [6–9]methods are conventionally adopted in the fabrication of MCIF. The first two have been widely used in the commercial production; while the latter one, in spite of showing greater potential to bring in more complex fiber design, takes more efforts and merely finds demonstration in lab currently. Commercial MCIFs usually contain from thousands up to nearly 100,000 cores with lattice defects kept below 0.1%. The typical resolution of MICF varies from several microns to tens of microns which is determined by the pitch of core and strength of crosstalk depending on wavelength. Fujikura product FIGH-30-650S [10], for example, can fully resolve the details of the 1950 USAF target at a wavelength of about 550 nm in a zero working distance. While at longer wavelengths, its imaging resolution declines with the rising of crosstal [7,8,10].

Numerical aperture (NA) of silica glass MCIF hardly exceeds 0.4 by pairing the highly germanium-doped and fluorine-doped silica glasses as the core and cladding materials [11]. Highly doped softglass materials are can offer an extensive selection range of NA [12,13], in spite of degraded transparency and relatively low use tempera-ture [14,15]. The state-of-the-art commercial fiber bundles, e.g. Fujikura (FIGH-10-500N, FIGH-10-350S) and Sumitomo (IGN-05/10), are composed of germanium-doped silica cores with a fluorine-doped common cladding with an NA of 0.35 ~ 0.39. Edmund Optics' rigid fiber bundles (NT53-846 and NT53-840) have an NA of 0.53 ~ 0.55 [16]. Recently a novel design of air-clad MCIF is proposed and fabricated at the University of Bath and the air-silica microstructure can bring down the effective index of cladding close to 1, and raise the NA of MCIF up to 1. The large NA helps MCIF effectively reduce the core size and pitch where the crosstalk still remains low [8]. However, the fabrication of such delicate fiber design makes it challenging to scale up the number of cores for a larger vision field.

In this paper, we report design, fabrication and characterization of high-resolution MCIF made of low-cost, commercial multi-component silicate glasses for fiber endoscopy application at ambient temperature

* Corresponding authors at: Key Laboratory of Materials for High Power Laser, Shanghai Institute of Optics and Fine Mechanics, Chinese Academy of Sciences, Shanghai 201800, China (F. Yu). State Key Laboratory of High-Temperature Gas Dynamics, Institute of Mechanics, Chinese Academy of Sciences, Beijing 100190, China (X. Lin).
E-mail addresses: yufei@siom.ac.cn (F. Yu), linxin_bit@imech.ac.cn (X. Lin).
[1] Authors make equal contribution

https://doi.org/10.1016/j.optlastec.2022.108650
Received 9 April 2022; Received in revised form 13 July 2022; Accepted 31 August 2022
Available online 12 September 2022

Table 1
Key parameters of H-ZK9B and H-K3 glasses.

	Refractive Index At 587.56 nm wavelength	Tg (℃)	Ts (℃)	Material absorption at 600 nm wavelength
H-K3	1.50463	537	609	1.739 dB/m
H-ZK9B	1.62041	663	704	0.869 dB/m

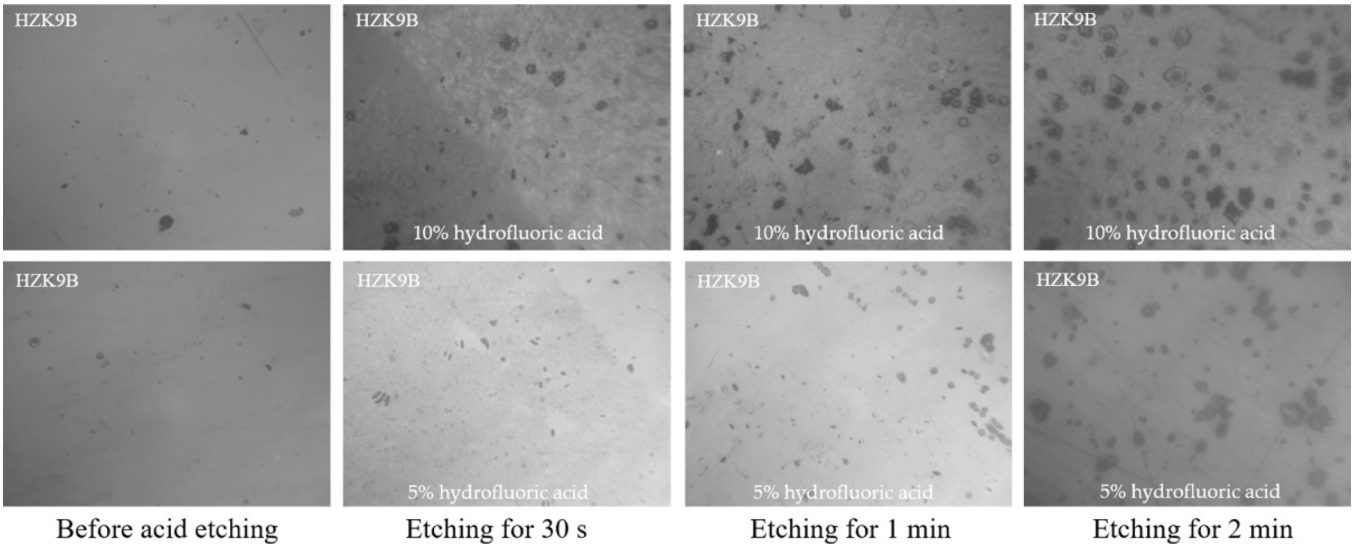

Fig. 1. Treated surfaces of H-ZK9B glass etched by hydrofluoric acid of different concentrations and for different dissolution times.

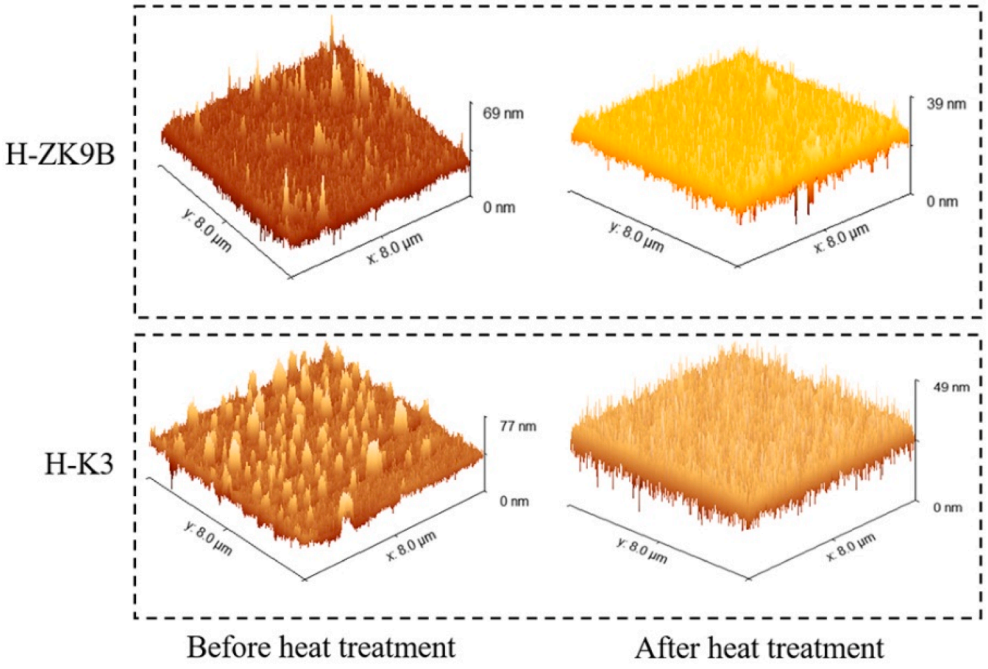

Fig. 2. Surfaces of two glass samples before and after heat treatment are characterized by AFM (Single-Chip AFM, nGauge, Canada).

of 260 ℃. H-ZK9B and H-K3 glass-es are used as core and cladding materials leading to a NA of 0.55. The applied three-size core design of MCIF is demonstrated an effective strategy to suppress the core-to-core crosstalk with a substantial improvement over the commercial state-of-the-art fiber bundles.

2. Glass preparation and test

H-ZK9B and H-K3 glasses are chosen for the balanced performances of spectral transparency, thermal expansion mismatching and manufacture cost (with basic parameters summarized in Table 1). Their relatively high transition temperatures allow MCIF to work at temperature of 260 ℃.

At 650 nm wavelength, the internal transmittance of 5 mm thick H-

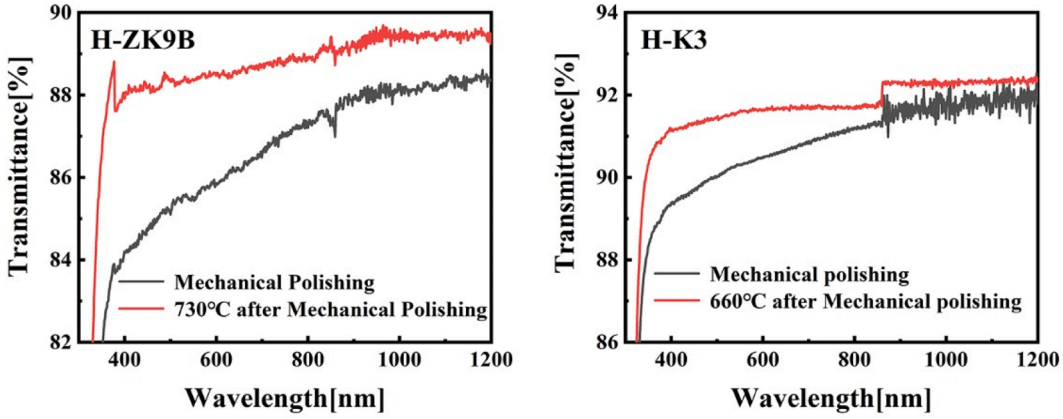

Fig. 3. Transmittance of glass samples was measured with a spectrophotometer (Perkin Elmer Lambda950) for different polishing conditions.

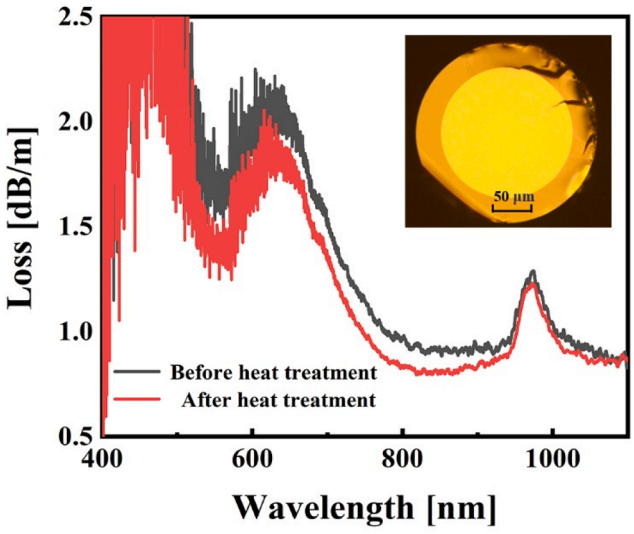

Fig. 4. Measured losses of multimode fibers made of glasses with and without heat treatment. The inset is one multimode fiber end under the optical microscope. The core diameter is 152 um and the fiber outer diameter is 210 um.

K3 glass is measured as 0.998, and 0.999 for H-ZK9B, corresponding to 1.739 dB/m and 0.869 dB/m respectively.

The stack-and-draw method uses rods and tubes of millimeters in diameter for fabrication. As the result, the raw glasses are machined and mechanical polished for preparation in the first place. Under a microscope, the mechanically polishing leaves a notable amount of pits and scratches on the glass surface, which would possibly cause defects of MCIF giving rise to strong scattering and high fiber loss. To remove the microscopic defects, further treatment of glass surface using chemical and thermal polishing are explored and compared.

2.1. Chemical polishing

Chemical polishing of host glasses is achieved by etching using hydrofluoric acid. Mechanically polished samples of H-ZK9B as the core glass material were cut into 2 cm long by 1 cm wide by 2 mm thick pieces. The hydrofluoric acid was diluted to 10% and 5% and immersed samples for 30 s, 1 min and 2 min respectively. The treated samples were then washed and cleaned by supersonic in the deionized water.

Fig. 1 compare glass samples under microscope before and after chemical etching and indicate that the surface roughness of samples become deteriorated by using HF etching. We attribute the ineffectiveness of chemical etching to the isotropic nature of wet etching as similarly reported in [17–19]. In the process of dissolution of uneven glass surface, the local defects with large curvature could suffer a quicker reaction dis-solution rate, resulting in the expansion and extension of scratches and pits.

2.2. Thermal polishing

Thermal polish of glass refers to the reduction of the surface roughness at high temperature close to the transition temperature, where the reduced viscosity in the surface of glass leads to the recovery of surface smoothness by surface tension [20,21]. In the thermal polishing treatment, mechanically polished glass samples were placed in an annealing furnace, where the temperature was ramped at a rate of 5 °C/hour. H-K3 and H-ZK9B glasses were annealed at 660 °C and 730 °C for 2 h respectively and then cooled down at a natural rate to the room temperature. Fig. 2 shows the measurement of surface roughness of two types of glasses before and after the thermal treatment using atomic force microscope. Thermal polishing effectively decreases the surface roughness of two glasses after heat treatment.

Fig. 3 shows the measured transmittance of the two glasses under different polishing conditions. The measured transmittance in the wavelength range from 350 nm to 1000 nm increases by 2% to 4% after the thermal polishing. Notably, a slight deformation of the glass samples was observed when the heating temperature was close to the transition temperature.

2.3. Loss of multimode optical fiber made of H-K3 and H-ZK9B glasses

To evaluate the loss of MCIF made of H-K3 and H-ZK9B, multimode optical fibers were fabricated by the stack-and-draw and characterized.

Two sets of rod and tube of same sizes were mechanically polished first. And one was then thermally treated. The two sets were stacked and drawn into two multimode optical fibers with the same core diameter of 152 um. The losses of two fibers were measured using the standard cutback method as shown in Fig. 4. It is demonstrated that the use of thermal polishing effectively reduces the fiber loss by 0.773 dB on average.

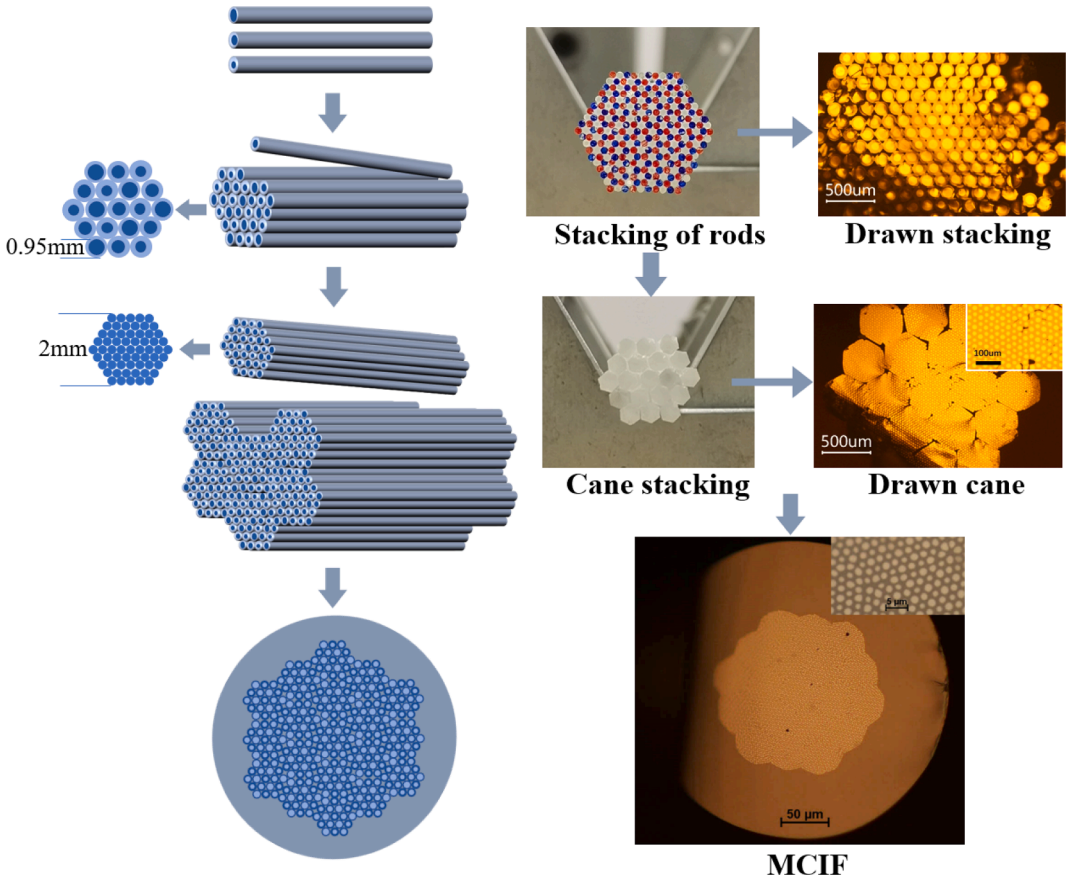

Fig. 5. ***Left***: Schematic of multiple-stack-and-draw method; and ***Right:*** pictures of stacking at each stage to fabricate MCIF. Rods of the first stacking units were stacked and drawn from raw glasses of H-K3 and H-ZK9. In the first stage of stacking, rods with different core sizes are painted in different colors to ensure no two preforms share the same core size in neighbour.

3. MCIF fabrication

The pursuit of higher resolution of MCIF demands higher density of cores and lower strength of crosstalk so that a higher NA is always favorable. In 2017, Stone and colleagues proposed the multi-stacking arrays of three-sized cores to effectively suppress the crosstalk where the NA was only around 0.2 [7]. In hexagonal stacking, the use of three-sized fiber preforms is the most economical to arrange MCIF design so that cores in the closest neighbour are different in diameter. The inter-core coupling is thus suppressed effectively to bring with the enhanced imaging quality of MCIF. We apply the three-sized core design in our MCIF and fabricate MCIF by a multi-stage stack-and-draw method as similarly described in [7,22].

Firstly, multimode optical fiber preforms were stacked and drawn from rods and tubes machined and polished from raw glasses into pieces of 1-meter length with an outer diameter of 950 μm. Three core-cladding ratios are 0.5, 0.61 and 0.72. As shown in Fig. 5, 271 elements of preforms were arranged and stacked into hexagonal arrays without identical cores in neighbor. We draw the first stacking into canes of 2 mm across as stacking units for the next stacking stage. Finally 19 canes were stacked, inserted into a jacket tube made of H-K3 glass and eventually drawn into MCIF. The obtained MCIF has an outer diameter of about 310 μm, and 5149 cores as "pixels". It is noted that air gaps between rods in the stacking were collapsed by applying vacuum in the fiber fabrication process. The deformation of claddings leads to the core size varying in a range from 1.05 μm to 1.8 μm as shown in Fig. 6.

4. Numerical simulation of inter-core coupling of MCIF

Deformation of cores in both shape and size can be found in both drawn cane and final MCIF in Fig. 5 because of malposition in the stacking and the vacuuming of gap in the drawing.

300 cores in total are selected from an area of the fabricated MCIF under a microscope, and the histogram of average core diameter (equivalent circle diameter of the same core area) distribution is shown in Fig. 6 (a). The deformation of fiber cores is attributed to the malposition and sliding in the stack-and-draw process. Fig. 6 (b)-(d) plot the calculated inter-core coupling efficiencies at 650 nm, 850 nm and 1000 nm given the statistical ranges of core diameters. It is noted that the inter-core coupling efficiency becomes constant due to the summed effect for a distance much longer than the beating length. Details of calculation refer to [23,24].

As Fig. 6 shows, the minimum coupling efficiency is calculated in the order of 10–13 between core 1 & core 3 at wavelength of 650 nm. The dash lines in Fig. 6 indicate the coupling efficiencies between cores of designed diameters Note that the maximum difference among average diameter of three cores is only about 600 nm. Therefore, the introduction of a three-sized-core design can well inhibit the coupling.

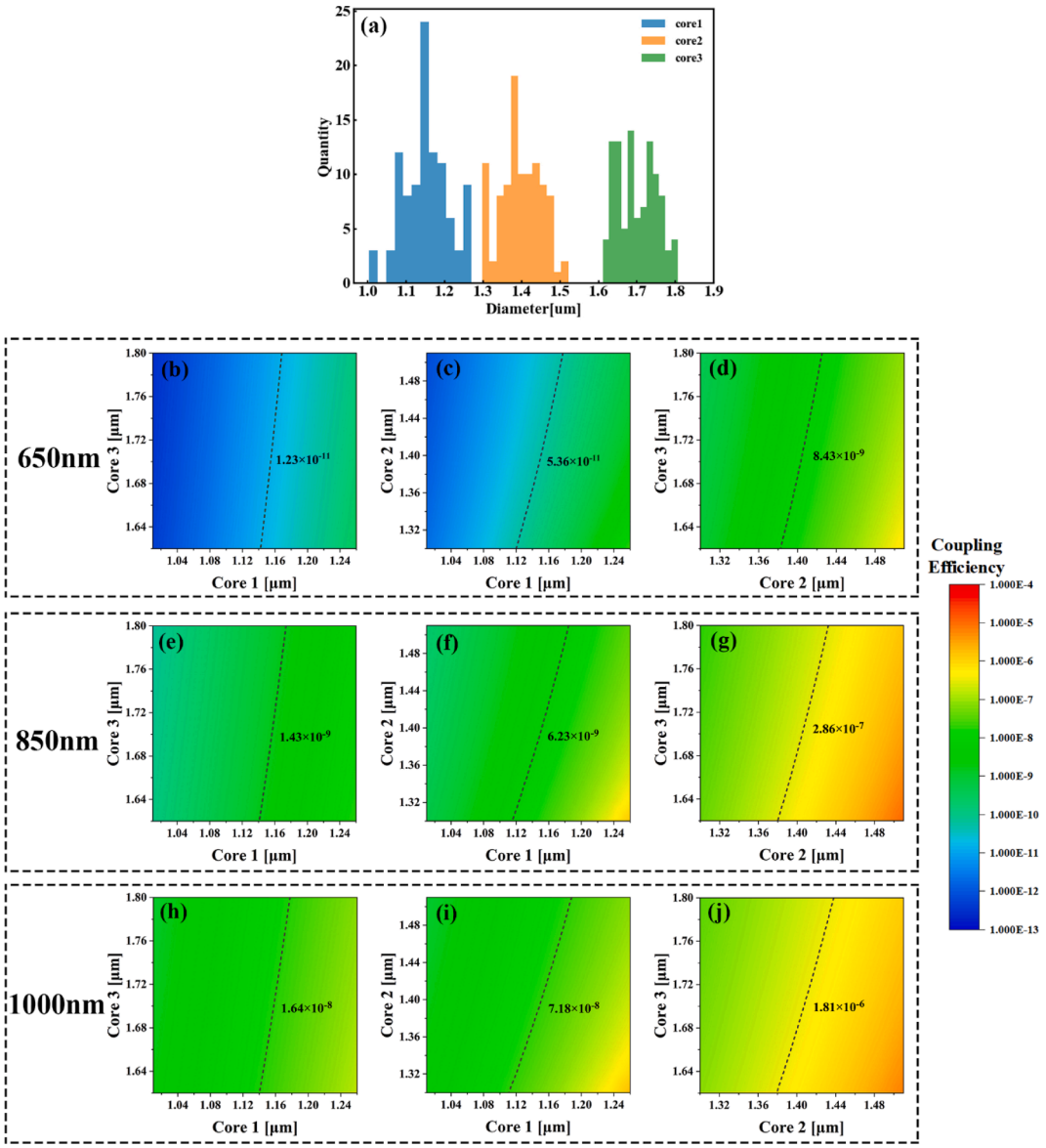

Fig. 6. . (a) Distribution of core diameters. (b)-(d) Coupling efficiency between core1&core3, core1&core2, core2&core3 at 650 nm. (e)-(g) at 850 nm (h)-(j) at 1000 nm. The dashed lines are calculated coupling efficiencies between cores of the designed diameters.

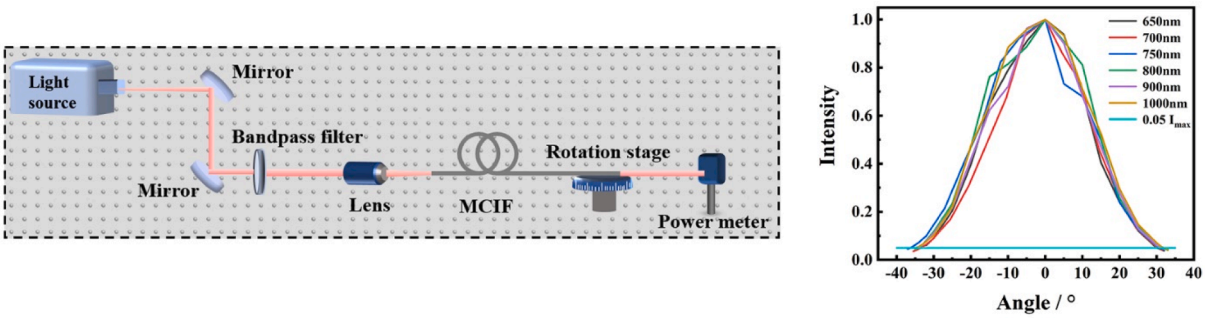

Fig. 7. ***Left:*** Schematic of NA measurement experiment. ***Right:*** The normalized distribution curve of measured intensity at different wavelengths. The intensity of 0.05 is marked in cyan.

Table 2
NA of MCIF at different wavelengths.

Wavelength	650 nm	700 nm	750 nm	800 nm	900 nm	1000 nm
NA	0.530	0.530	0.552	0.541	0.548	0.548

5. MCIF characterization

5.1. Numerical aperture

NA of MCIF was characterized (as shown in Fig. 7) by measuring the far-field intensity pattern out of fiber end at various wavelengths. A broadband light source was filtered by an bandpass filter(series of Thorlabs FKB-VIS-1 and FKB-IR-10 filter set) and launched into a 0.8 m length of fiber by using a high NA microscope objective lens (Olympus RMS40X, NA = 0.65). The distal end of MCIF was mounted on a high precision rotation stage before a power meter. When rotating the stage, we obtained the intensity distribution as a function of emission angle. The NA was determined by measuring the rotation angle where the intensity falls above 5 % of the maximum [25–27]. The NA values at different wavelengths are summarized in Table 2. The maximum NA of MCIF was 0.552 at 750 nm.

5.2. Resolution of imaging at zero working distance

We use the 1951 USAF test target to evaluate the resolution of MCIF. MCIF was cut in about 1 m long piece with both ends polished. The USAF target was placed against one end of MCIF and illuminated by the homemade optical fiber supercontinuum source as shown in Fig. 8. The output at the other end of MCIF was imaged on a CCD camera (Image Source, DMK23U74) by a lens. Different bandpass filters (series of Thorlabs FKB-VIS-1 and FKB-IR-10 filter set) were used in the experiment.

In the experiment, MCIF was kept straight and the seventh group of the USAF test target could be fully resolved at visible wavelengths and shorter wavelengths in the near-infrared (as shown in Fig. 9), corresponding to a resolution of 228 line pairs per millimeter, or namely a pitch of 2.19 um. In the near-infrared spectral region, the image became blurred at 900 nm and beyond, owing to the rising of inter-core coupling strength at long wavelengths. The brightness variation of MCIF cores is found in the imaging with all three fibers. In our MCIF, such difference is found more significant which we attribute to the dependence on loss that a larger core is usually found with a lower attenuation.

We tested our MCIF performance under bend by rewinding the fiber in one loop of different diameter to characterize the imaging resolution under bend. Fig. 10 shows the imaging of the UASF target by our MCIF under different bending radius from 8.93 cm to 1.48 cm at 650 nm. In the imaging test under bend, MCIF breaks at a bend radius around 1 cm, where no degradation of imaging is observed. Bend resistant imaging of MCIF could be favorable for practical medical endoscope applications, and it reported that a bending radius of at least 5 cm is required for MCIF to enter the upper lobe of the human lung [22].

6. Conclusions

In this paper, we demonstrate design and fabrication of high NA MCIF using cost-economic softglasses of H-K3 and H-ZK9. Compared with the current state-of-the-art commercial fiber bundle, our fiber shows a comparable imaging resolution but stronger bend resistance. At wavelengths from 550 nm to 900 nm, our fibers can resolve the smallest elements in the USAF targets corresponding to a resolution of 2.19 um. Under a bending radius of 1.48 cm, the imaging by MCIF shows no degradation. The broadband high resolution and bend resistant imaging performance make our MCIF a promising candidate for practical applications in fiber endoscopy.

All data underlying the results presented in this paper can be found at [28].

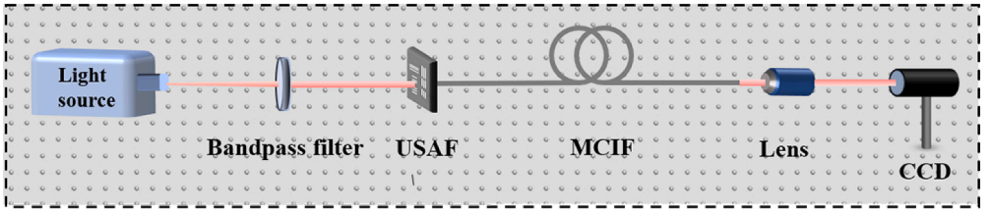

Fig. 8. Schematic MCIF imaging test at a zero working distance.

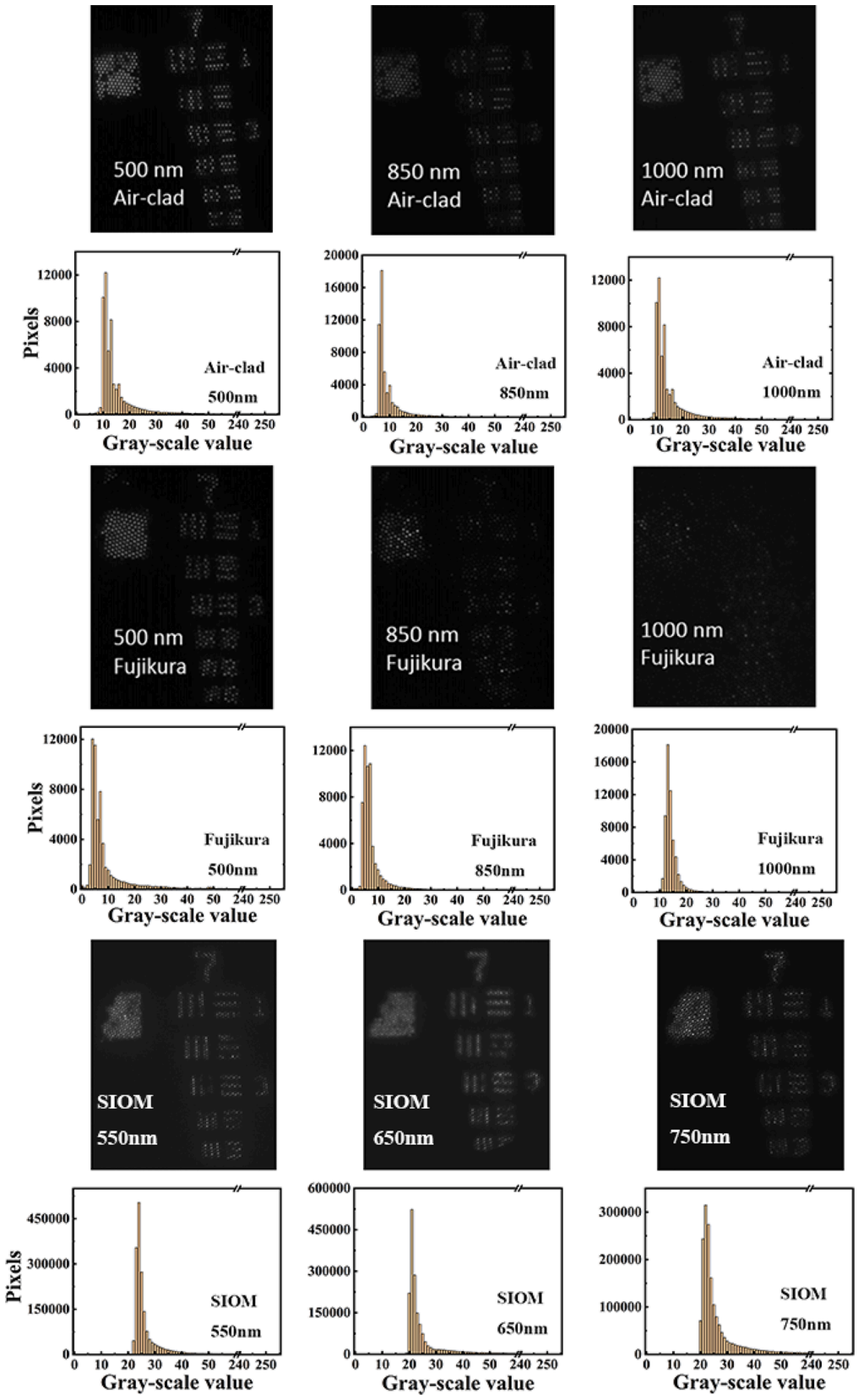

Fig. 9. Zero-working distance imaging of the USAF target by using three types of image fibers. Fujikura FIGH-30-650S and Air-clad imaging fiber at the University of Bath, reprinted from [8]; and cropped so that the imaging of USAF test target group 7 are all kept only. Illumination on USAF test target is carefully adjusted in the experiment so that the images taken by MCIF present similar grey level distributions to the ones by Fujikura and UOB imaging fibers for the convenience of comparison.

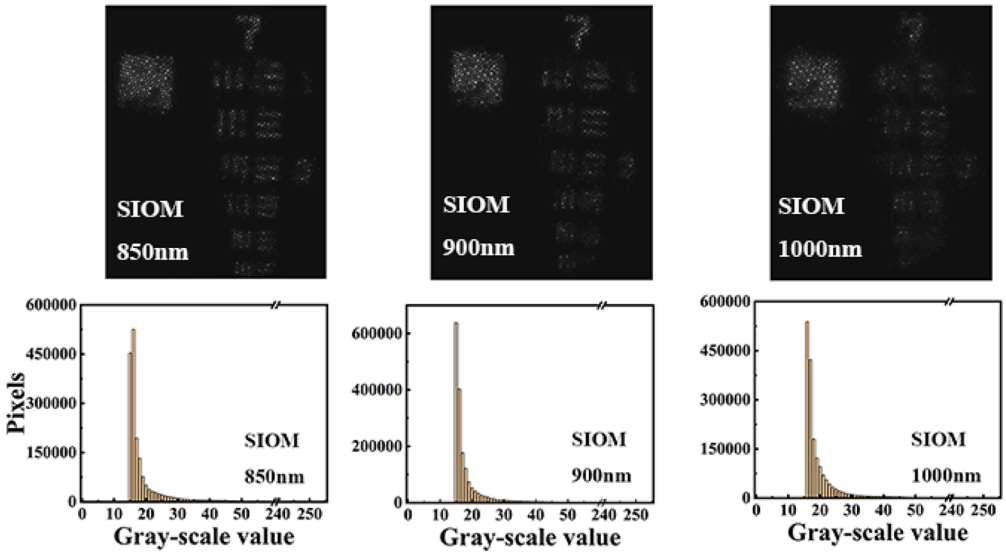

Fig. 9. (*continued*).

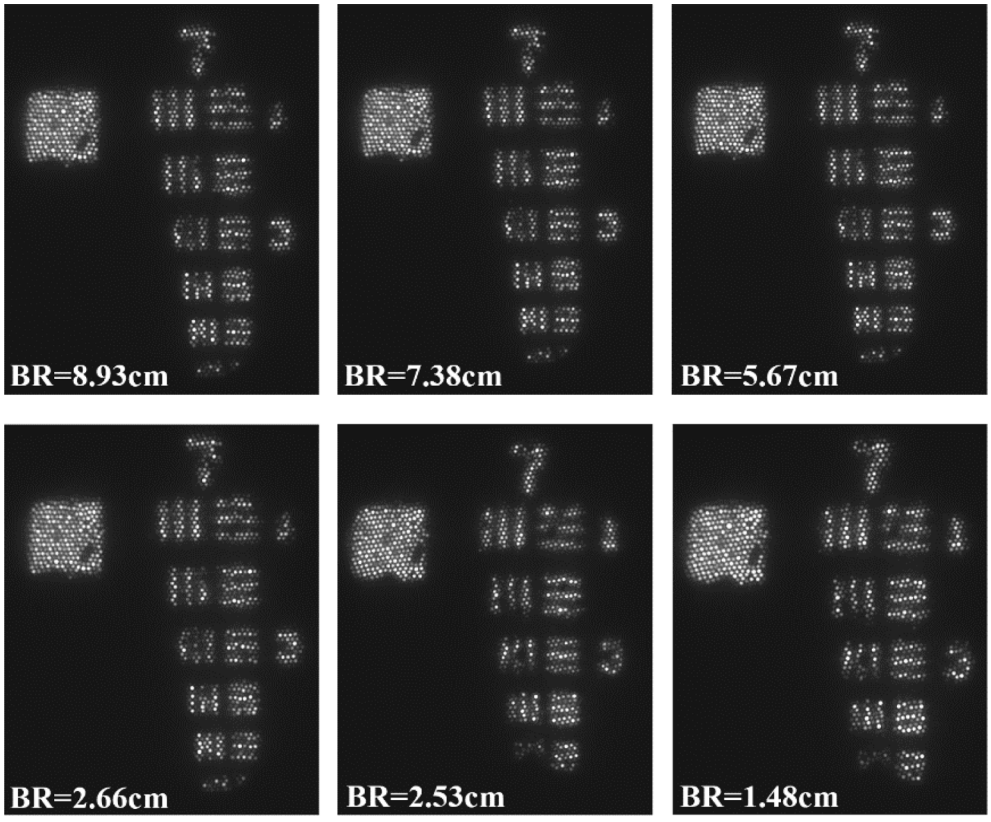

Fig. 10. The imaging of UASF targe by our MCIF under different bending radii at 650 nm wavelength.

Declaration of Competing Interest

The authors declare that they have no known competing financial interests or personal relationships that could have appeared to influence the work reported in this paper.

Acknowledgement

This work is supported by the : Chinese Academy of Sciences (Pioneer Hundred Talents Program, ZDBS-LYJSC020); State Key Laboratory of High Temperature Gas Dynamics (2021KF13).

References

[1] I. Gannot, A. Seki, K. Iwai, T. Katagiri, Y. Matsuura, Photoacoustic imaging by using a bundle of thin hollow-optical fibers. Proceedings of the Optical Fibers and Sensors for Medical Diagnostics and Treatment Applications XVI, 2016.

[2] J. Zhao, Y. Sun, Z. Zhu, J.E. Antonio-Lopez, R.A. Correa, S. Pang, A. Schülzgen, Deep learning imaging through fully-flexible glass-air disordered fiber, ACS Photonics 5 (2018) 3930–3935, https://doi.org/10.1021/acsphotonics.8b00832.

[3] X. Hu, J. Zhao, J.E. Antonio-Lopez, S. Fan, R. Amezcua Correa, A. Schulzgen, Robust imaging-free object recognition through anderson localizing optical fiber, J. Lightwave Technol. (2020) 1, https://doi.org/10.1109/jlt.2020.3029416.

[4] S. Lei, Large cross-section fiber bundle and its application, J. Appl. Opt. (2000).

[5] P. Falkenstein, C.D. Merritt, B.L. Justus, Fused preforms for the fabrication of photonic crystal fibers, Opt. Lett. 29 (2004) 1858–1860, https://doi.org/10.1364/ol.29.001858.

[6] T. Kobayashi, T. Katagiri, Y. Matsuura, Multi-element hollow-core anti-resonant fiber for infrared thermal imaging, Opt. Express 24 (2016) 26565–26574, https://doi.org/10.1364/OE.24.026565.

[7] J.M. Stone, H.A. Wood, K. Harrington, T.A. Birks, Low index contrast imaging fibers, Opt. Lett 42 (2017) 1484–1487, https://doi.org/10.1364/OL.42.001484.

[8] H.A.C. Wood, K. Harrington, T.A. Birks, J.C. Knight, J.M. Stone, High-resolution air-clad imaging fibers, Opt. Lett 43 (2018) 5311–5314, https://doi.org/10.1364/OL.43.005311.

[9] D. Pysz, I. Kujawa, R. Stępień, M. Klimczak, A. Filipkowski, M. Franczyk, L. Kociszewski, J. Buźniak, K. Haraśny, R. Buczyński, Stack and draw fabrication of soft glass microstructured fiber optics, Bull. Polish Acad. Sci. Tech. Sci. 62 (2014).

[10] H.A.C. Wood, K. Harrington, J.M. Stone, T.A. Birks, J.C. Knight, Quantitative characterization of endoscopic imaging fibers, Opt Express 25 (2017) 1985–1992, https://doi.org/10.1364/OE.25.001985.

[11] X.P. Chen, K.L. Reichenbach, C. Xu, Experimental and theoretical analysis of core-to-core coupling on fiber bundle imaging, Opt. Express 16 (2008) 21598–21607, https://doi.org/10.1364/OE.16.021598.

[12] B. Morova, N. Bavili, O. Yaman, B. Yigit, M. Zeybel, M. Aydın, B. Dogan, R. Kasztelanic, D. Pysz, R. Buczynski, Fabrication and characterization of large numerical aperture, high-resolution optical fiber bundles based on high-contrast pairs of soft glasses for fluorescence imaging, Opt. Express 27 (2019) 9502–9515.

[13] R. Stepien, J. Cimek, D. Pysz, I. Kujawa, P. Golebiewski, G. Stepniewski, K. Orlinski, R. Buczynski, R. Kasztelanic, High-contrast lead-free pair of soft glasses for large numerical aperture imaging bundles, Opt. Mater. Express 10 (2020) 1891–1910, https://doi.org/10.1364/ome.394918.

[14] B. Bureau, S. Maurugeon, F. Charpentier, J.L. Adam, C. Boussard-Pledel, X. H. Zhang, Chalcogenide glass fibers for infrared sensing and space optics, Fiber Integr. Opt. 28 (2009) 65–80, https://doi.org/10.1080/01468030802272542.

[15] L.N. Butvina, O.V. Sereda, E.M. Dianov, N.V. Lichkova, V.N. Zagorodnev, Singlemode photonic crystal fiber for the middle infrared. Proceedings of the Conference on Enabling Photonics Technologies for Defense, Security, and Aerospace Application III, Orlando, FL, Apr 09-10, 2007.

[16] J.-H. Han, J.U. Kang, Effect of multimodal coupling in imaging micro-endoscopic fiber bundle on optical coherence tomography, Appl. Phys. B 106 (2012) 635–643.

[17] G.J. Exarhos, M.D. Feit, V.E. Gruzdev, T.I. Suratwala, L.L. Wong, D. Ristau, M. J. Soileau, W.A. Steele, P.E. Miller, C.J. Stolz, et al., Modeling wet chemical etching of surface flaws on fused silica. Proceedings of the Laser-Induced Damage in Optical Materials, 2009, 2009..

[18] L. Wong, T. Suratwala, M.D. Feit, P.E. Miller, R. Steele, The effect of HF/NH4F etching on the morphology of surface fractures on fused silica, J. Non-Cryst. Solids 355 (2009) 797–810, https://doi.org/10.1016/j.jnoncrysol.2009.01.037.

[19] C. Li, Y. Sun, X. Song, X. Zhang, Z. Shi, F. Wang, X. Ye, S. Chen, L. Sun, J. Huang, et al., Capping a glass thin layer on the etched surface via plasma chemical vapor deposition for improving the laser damage performance of fused silica, Opt Express 27 (2019) 2268–2280, https://doi.org/10.1364/OE.27.002268.

[20] C. Weingarten, A. Schmickler, E. Willenborg, K. Wissenbach, R. Poprawe, Laser polishing and laser shape correction of optical glass, J. Laser Appl. 29 (2017).

[21] A. Ostendorf, C. Kulik, P.O. Wiechell, Automatic control of a thermal based polishing process for aspherical optics, in: Proceedings of the Conference on Optical Fabrication, Testing, And Metrology, St Etienne, FRANCE, Sep 30-Oct 03, 2003, pp. 69–79.

[22] H.A.C. Wood, Novel Fibres for Endoscopy, University of Bath, 2019.

[23] J. Popp, N. Ortega-Quijano, W. Drexler, F. Fanjul-Vélez, I. Salas-García, V. V. Tuchin, D.L. Matthews, Ó.R. Hernández-Cubero, J.L. Arce-Diego, Analysis of optical crosstalk in flexible imaging endoscopes based on multicore fibers. Proceedings of the Biophotonics: Photonic Solutions for Better Health Care II, 2010.

[24] N. Ortega-Quijano, F. Fanjul-Vélez, J.L. Arce-Diego, Optical crosstalk influence in fiber imaging endoscopes design, Opt. Commun. 283 (2010) 633–638, https://doi.org/10.1016/j.optcom.2009.10.075.

[25] N.A. Issa, High numerical aperture in multimode microstructured optical fibers, Appl. Opt. 43 (2004) 6191–6197.

[26] J. Pniewski, G. Stepniewski, R. Kasztelanic, B. Siwicki, D. Pierscinska, K. Pierscinski, D. Pysz, K. Borzycki, R. Stepien, M. Bugajski, High numerical aperture large-core photonic crystal fiber for a broadband infrared transmission, Infrared Phys. Technol. 79 (2016) 10–16.

[27] W.J. Wadsworth, R.M. Percival, G. Bouwmans, J.C. Knight, T.A. Birks, T.D. Hedley, P.S.J. Russell, Very high numerical aperture fibers, IEEE Photonics Technol. Lett. 16 (2004) 843–845.

[28] http://doi.org/10.57760/sciencedb.02589. https://www.scidb.cn/s/RNv2mq.